applied sciences

MDPI

Article

Tailoring Asymmetric Lossy Channels to Test the Robustness of Mesoscopic Quantum States of Light

Alessia Allevi [1,2,*,†] **and Maria Bondani** [2,†]

[1] Department of Science and High Technology, University of Insubria, Via Valleggio 11, I-22100 Como, CO, Italy
[2] Institute for Photonics and Nanotechnologies, CNR, Via Valleggio 11, I-22100 Como, CO, Italy; maria.bondani@uninsubria.it
* Correspondence: alessia.allevi@uninsubria.it; Tel.: +39-031-238-6253
† These authors contributed equally to this work.

Received: 23 November 2020; Accepted: 16 December 2020; Published: 19 December 2020

Abstract: In the past twenty years many experiments have demonstrated that quantum states of light can be used for secure data transfer, despite the presence of many noise sources. In this paper we investigate, both theoretically and experimentally, the role played by a statistically-distributed asymmetric amount of loss in the degradation of nonclassical photon-number correlations between the two parties of multimode twin-beam states in the mesoscopic intensity regime. To be as close as possible to realistic scenarios, we consider two different statistical distributions of such a loss, a Gaussian distribution and a log-normal one. The results achieved in the two cases show to what extent the involved parameters, both those connected to loss and those describing the employed states of light, preserve nonclassicality.

Keywords: mesoscopic quantum states of light; nonclassical photon-number correlations; lossy transmission channels

1. Introduction

Since the seminal paper in which Bennett and Brassard dealt with the transmission of quantum states and cryptographic keys through 0.3-m-long free-space air [1], Quantum Communication over long distances has received a lot of interest. In the past two decades, many experiments have been performed using both optical fibers [2–4] and free-space [5–7] channels. Starting from the successful implementation of ground-to-ground atmospheric links [8,9], some most recent experiments have also involved a satellite link [10–12]. Despite all these results, the development of a real global communication network in free-space propagation is still prevented by the atmospheric turbulence, which acts as a temporal and spatial variation of the air refraction index, thus varying the transmittance of the links in a turbulent way. In order to understand the behavior of quantum states of light propagating through atmospheric links, a deep investigation of quantum channels is required [13]. In this respect, quite recent works have introduced different fluctuation loss models capable of accurately describe some experimental results [14,15]. At the same time, it is also important to investigate which kinds of quantum states and nonclassical features are more robust against atmospheric fluctuations and can survive under specific conditions [16]. Until now, most experiments have been implemented at the single-photon level. Recently, we have realized an experiment involving mesoscopic twin-beam states, in which signal and idler were affected by different amounts of loss distributed according to specific statistical distributions [17]. In particular, we have investigated how nonclassicality changes as a function of the mean value of the distributions for fixed values of their standard deviation. Here we face the problem from a different point of view, that is we

consider the case in which the standard deviation of the distribution is varied and the mean value of the distribution is fixed. At variance with the previous paper, we deeply analyze the behavior of nonclassicality by choosing worse and worse situations, down to very low and very noisy transmission-efficiency values. For all the chosen values of the parameters, we consider two possible transmittance distributions, namely the log-normal distribution [18,19], which is typically used to describe very turbulent transmission channels, and the Gaussian distribution, which can be exploited to model free-space channels under specific weather conditions [20]. To investigate the nonclassicality of the generated twin beams, which are entangled in the number of photons, we consider the noise reduction factor (R). Indeed, it has been demonstrated that $R < 1$ represents a sufficient criterion for entanglement in the case of bipartite Gaussian states [21]. Actually, many other nonclassicality criteria exist and have been proposed over the years [22–27]. However, not all of them can be easily applied to any experimental situation. Some of them, such as those based on separability criteria, require the full reconstruction of the state under investigation. On the contrary, the noise reduction factor can be calculated from experimental data in a more direct way, also because it can be defined in terms of measurable quantities [28] (see the next section). The obtained results shed light on the different behavior of nonclassicality according to the chosen distribution of the transmission efficiency and on the evolution of such a behavior as a function of the different parameters. To be more exhaustive, in this work we also investigate the role played by the mean number of photons per mode of the employed quantum states in the entanglement degradation process.

Our analysis can give some useful hints not only for the exploitation of quantum states in communication protocols, but also for their application in different contexts, such as for imaging protocols [29–31].

2. Materials and Methods

2.1. Statistical Distributions of the Transmittance Coefficient

The transmission of light through a linear medium can be described by a wavelength- and polarization-dependent transmission coefficient. However, noise effects, such as absorption, depolarization, dephasing and scattering, can occur simultaneously, thus determining a variable transmittance coefficient or, more properly, a statistically-distributed transmittance coefficient. The situation is even more critical when the transmitted light is not represented by a single state but rather by a multipartite one. Indeed, in such a case, the different components of the state can experience different transmission efficiencies. This fact can determine the degradation of the correlations existing among the parties. It is thus crucial to quantify the amount of degradation in order to verify if the employed multipartite state is still useful for applications or not [32]. For instance, in the case of correlated bipartite systems, both classical and quantum, it is possible to get a fair estimation of the occurrence of degradation in terms of the noise reduction factor R, which is defined as

$$R = \frac{\sigma^2(n_1 - n_2)}{(\langle n_1 \rangle + \langle n_2 \rangle)}, \tag{1}$$

in which $\sigma^2(n_1 - n_2)$ is the variance of the distribution of the photon-number difference between the two parties, while $(\langle n_1 \rangle + \langle n_2 \rangle)$ is the shot-noise-level, that is the value of $\sigma^2(n_1 - n_2)$ in the case of coherent states having mean values $\langle n_1 \rangle$ and $\langle n_2 \rangle$.

Typically, the noise reduction factor is used to test the nonclassicality of quantum states of light, $R < 1$ being a sufficient condition for entanglement be expressed in terms of measurable quantities, such as the "detected" number of photons. As an example, in the case of multimode twin-beam states, the measured noise reduction factor reads [33]

$$R = 1 - \frac{2\sqrt{\eta_1 \eta_2}\sqrt{\langle m_1 \rangle \langle m_2 \rangle}}{\langle m_1 \rangle + \langle m_2 \rangle} + \frac{(\langle m_1 \rangle - \langle m_2 \rangle)^2}{\mu(\langle m_1 \rangle + \langle m_2 \rangle)} \tag{2}$$

and the condition $R < 1$ proves the existence of sub-shot-noise correlations between the two parties. In Equation (2), $\langle m_1 \rangle$ and $\langle m_2 \rangle$ are the mean number of detected photons in the two arms of twin beam, μ is the number of modes, and η_1 and η_2 are the detection efficiencies. In Ref. [17] we considered the presence of an asymmetric loss in the two arms of twin beam, and defined $\langle m_1 \rangle = \langle m \rangle = \eta \langle n \rangle$ and $\langle m_2 \rangle = \langle m \rangle t = \eta \langle n \rangle t$ ($t \in (0,1)$). The expression for R modifies as:

$$R = 1 - \frac{2\eta t}{1+t} + \frac{(1-t)^2}{(1+t)} m_\mu, \tag{3}$$

in which $m_\mu = \langle m \rangle / \mu$ is the mean number of photons per mode. As stated above, in realistic situations, the asymmetric transmittance coefficient t is not constant but rather statistically distributed. In this case, by following the procedure presented in Ref. [17], it is still possible to find an analytic expression for the noise reduction factor R, that is

$$R = 1 - \frac{2\eta \langle t \rangle}{1+\langle t \rangle} + \frac{1-\langle t \rangle)^2}{1+\langle t \rangle} m_\mu + \left(\langle m \rangle + m_\mu \right) \frac{\sigma^2(t)}{1+\langle t \rangle}. \tag{4}$$

We notice that in Equation (4) only the first two moments of the statistics of t are involved, namely $\langle t \rangle$ and $\sigma^2(t)$. This makes the investigation of the degradation of entanglement for twin-beam states particularly straightforward once the two moments of the distribution of t are known (or can be calculated). As an example, in Figure 1 we show a 3D plot of R as a function of $\langle t \rangle$ and $\sigma(t)$ for $\eta = 0.145$, $\langle m \rangle = 2.23$ and $m_\mu = 0.04$, which represent typical experimental values.

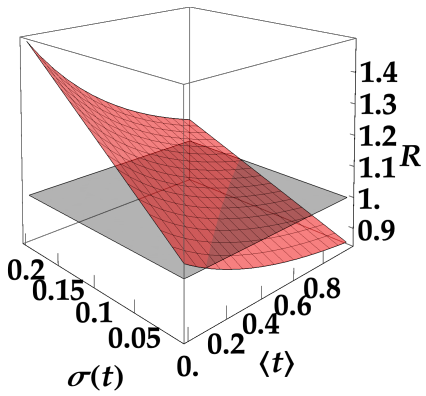

Figure 1. Theoretical expectation, according to Equation (4), of R (red surface) as a function of $\langle t \rangle$ and of $\sigma(t)$ for $\eta = 0.145$, $\langle m \rangle = 2.23$ and $m_\mu = 0.04$. The gray surface at $R = 1$ represents the boundary plane between classical and nonclassical correlations.

As expected, the observation of nonclassical correlations becomes very difficult both at low values of $\langle t \rangle$ and at values of $\sigma(t)$ exceeding a threshold that depends on $\langle t \rangle$.

In the following, we consider two loss distributions that are involved in the propagation process of light through media. In particular, we deal with Gaussian and log-normal distributions. The Gaussian distribution of t can be expressed as

$$P_g(t) = \frac{1}{\sqrt{2\pi}\sigma_0} \exp\left[\frac{-(t-t_0)^2}{2\sigma_0^2} \right], \tag{5}$$

where t_0 and σ_0 are the mean value and the standard deviation for t $\in (-\infty, +\infty)$, while the log-normal distribution is usually defined as

$$P_{\ln}(t) = \frac{1}{\sqrt{2\pi}\sigma_\xi t} \exp\left[\frac{-[-\xi + \ln(t)]^2}{2\sigma_\xi^2} \right], \tag{6}$$

in which $\xi \in \Re$ is the so-called location parameter and $\sigma_\xi > 0$ is the scale parameter. Both parameters are linked to the mean value and the standard deviation of the distribution for $t \in (0, +\infty)$: $t_0 = \exp[\xi + \sigma_\xi^2/2]$ and $\sigma_0^2 = (\exp[2\xi + \sigma_\xi^2])(-1 + \exp[\sigma_\xi^2])$.

For the specific application we are considering, the transmittance coefficient t is limited to the interval (0,1), which means that the distributions in Equations (5) and (6) must be properly normalized in the interval (0,1). The resulting probabilities can be expressed through closed formulas and the same holds for the first two moments of the distributions, $\langle t \rangle$ and $\sigma(t)$.

In order to appreciate the differences between the two distributions, in Figure 2 we show some examples. We observe that, in general, at increasing the standard deviation, the discrepancies between Gaussian and log-normal distributions become more evident, since the log-normal distribution gets more asymmetric, while the Gaussian one remains symmetric. Moreover, comparing the two distributions for a given choice of standard deviation and mean value shows that for small mean values of t_0 (see panels (a) and (b)) and large values of σ_0 (see magenta curves) the log-normal distribution is confined in the region corresponding to small values of t (dashed line), while the Gaussian one is uniformly distributed all over the range (0,1) (solid line). On the contrary, for large mean values of t_0 (see panels (c) and (d)) and large values of σ_0 (see magenta curves) the Gaussian distribution has a longer tail towards small values of t than the log-normal one. At variance with these conditions, in all panels for small values of σ_0 (see black curves) the two distributions are more confined and more similar.

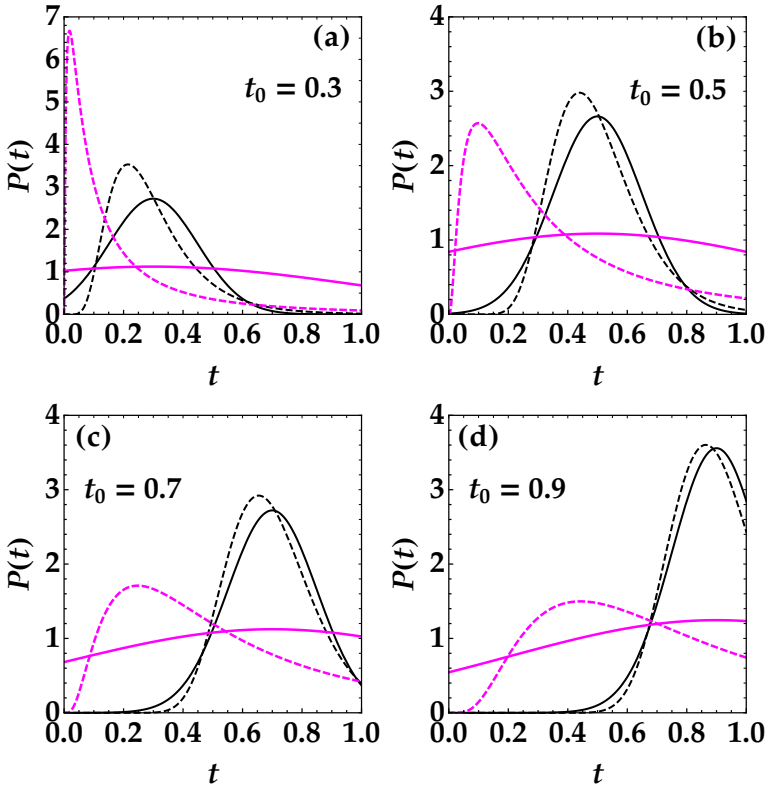

Figure 2. Gaussian (solid lines) and log-normal (dashed lines) probability distributions of t in the interval (0, 1). The four panels (**a**–**d**) correspond to different choices of the mean value t_0 of the distributions, as indicated in the label on top of each panel. Inside each panel, the different colors correspond to different choices of the standard deviation: $\sigma_0 = 0.15$ is represented in black, while $\sigma_0 = 0.7$ in magenta.

Before presenting the results of our investigation, we summarize the main features of the experimental implementation and explain the method used to prepare the data according to the specific distributions.

2.2. Experimental Setup and Data Preparation

A sketch of the employed experimental setup in shown in Figure 3. The fundamental (at 1047 nm) and the third harmonic (at 349 nm) of a Nd:YLF laser (IC-500, High Q Laser, Rankweil, Austria and 2003) regeneratively amplified at 500 Hz are sent to a $\beta-$barium-borate crystal (BBO1, cut angle = 37°, 8-mm long) in order to produce the fourth-harmonic (at 262 nm) field by noncollinear sum-frequency generation. The generated beam is used to pump spontaneous parametric downconversion in a second BBO (BBO2, cut angle = 46.7°, 6-mm long) crystal.

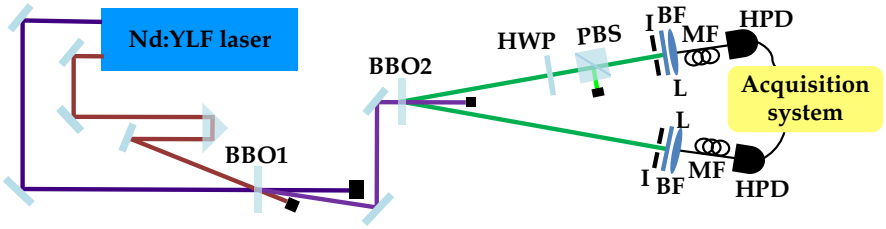

Figure 3. (Color online) Sketch of the experimental setup. See the text for details.

Two twin portions at frequency degeneracy are selected both spatially and spectrally by means of two irises (I) and two bandpass filters (BF), respectively. The filtered portions are then focused into two multimode fibers (600-μm-core diameter) and delivered to two hybrid photodetectors (HPD, mod. R10467U-40, Hamamatsu Photonics, Hamamatsu City, Japan and 2010). These are photon-number-resolving detectors endowed with a partial photon-number-resolving capability and a good linearity up to 100 photons. Each detector output is amplified, synchronously integrated and digitized. As extensively explained in previous papers, by applying a self-consistent method to each detector output it is possible to have access to detected photons and thus to the statistical properties of the measured states [33,34].

In order to introduce a variable transmittance coefficient (from 0 to 1) only in one arm of the twin-beam state, a half-wave plate (HWP) followed by a polarizing cube beam splitter (PBS) is inserted in that arm. During the measurements, the half-wave plate is rotated in steps of 2° and 50,000 acquisitions are saved for each angle value.

To build a given distribution $P(t)$ of the transmission coefficient, for each measured value t_i in the interval (0,1) we select a dataset of $P(t_i)$ elements on both arms and join all the chosen datasets preserving the correspondence of the single data in the two arms. In such a way, the statistics of light in the arm without variable transmittance remains unchanged, while that on the other arm gets modified. This determines a degradation of the nonclassical photon-number correlations between the two arms, which can be quantified by evaluating the noise reduction factor.

Note that this procedure allows us to check, starting from the same datasets, the effect of different distributions of t by simply changing $P(t)$ and choosing different values of t_0 and σ_0.

3. Results

At variance with Ref. [17], in which we focused our attention on the possibility of keeping observing nonclassicality in the presence of an asymmetric loss between the two parties of the twin-beam states, here we aim at finding the limits imposed by the parameters that describe the transmittance statistics, both for the Gaussian and the log-normal distributions. According to Equation (4), the noise reduction factor is a function of the first two moments of the distribution of t, independent of the considered distribution. This means that by choosing the same mean value $\langle t \rangle$ and the same standard deviation $\sigma(t)$, the Gaussian and the log-normal distributions act in the same way. On the contrary, if we consider the values of t_0 and σ_0 over the entire domains, we expect different results. To better emphasize this point, in panel (a) of Figure 4 we show, as contour plot, the difference $\langle t \rangle_{\mathrm{GAUSS}} - \langle t \rangle_{\mathrm{LOG}}$ between the mean value $\langle t \rangle$ of the normalized Gaussian distribution and that of the

normalized log-normal distribution as a function of t_0 and σ_0, while in panel (b) of Figure 4 we do the same for the standard deviation $\sigma(t)$, namely we plot the difference $\sigma(t)_{\mathrm{GAUSS}} - \sigma(t)_{\mathrm{LOG}}$. In panel (a) (panel (b)), the pink region corresponds to values of $\langle t\rangle_{\mathrm{GAUSS}} - \langle t\rangle_{\mathrm{LOG}}$ ($\sigma(t)_{\mathrm{GAUSS}} - \sigma(t)_{\mathrm{LOG}}$) larger than 0, the gray region to values lower than 0, and the black-dashed line dividing the pink region from the gray one corresponds to the condition $\langle t\rangle_{\mathrm{GAUSS}} - \langle t\rangle_{\mathrm{LOG}} = 0$ (panel (a)), and to the condition $\sigma(t)_{\mathrm{GAUSS}} - \sigma(t)_{\mathrm{LOG}} = 0$ (panel (b)). As it can be noticed by comparing the two panels, it is not possible to find a set of t_0 and σ_0 values corresponding to equal values of $\langle t\rangle$ and $\sigma(t)$ for the two distributions, unless one considers sparse choices of t_0 and σ_0 for $\sigma_0 < 0.05$.

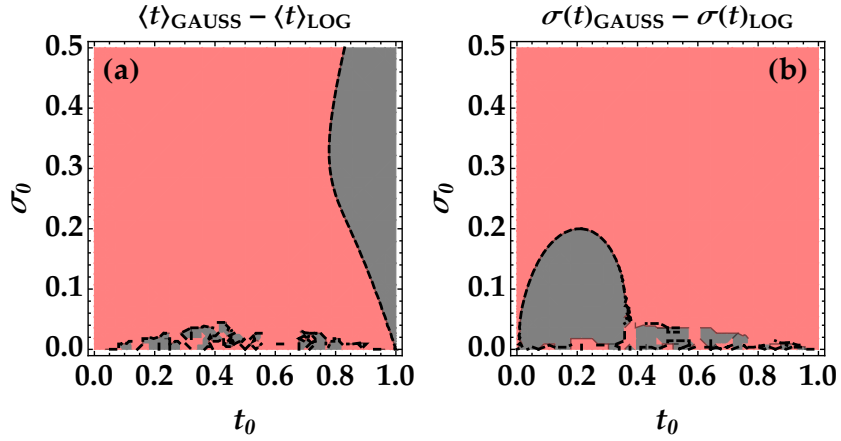

Figure 4. Panel (**a**): Contour plot of the difference $\langle t\rangle_{\mathrm{GAUSS}} - \langle t\rangle_{\mathrm{LOG}}$ of the Gaussian and log-normal distributions defined over the interval (0,1) as a function of the mean value t_0 and of the standard deviation σ_0 of the same distributions defined over the entire domain. Panel (**b**): The same as (**a**) for the difference $\sigma(t)_{\mathrm{GAUSS}} - \sigma(t)_{\mathrm{LOG}}$. In both panels, the black-dashed line corresponds to the condition in which the difference is equal to 0, the pink region to values larger than 0 and the gray region to values lower than 0.

For the above reasons, a direct comparison between the distributions could be not essential. On the contrary, it can be more interesting, for each one of the two distributions separately, to investigate the survival of nonclassical correlations as a function of its first two moments.

In particular, it is straightforward to deal with the expressions defined over the entire domain and their corresponding moments by considering the link among $\langle t\rangle$ and $\sigma(t)$ in Equation (4) to t_0 and σ_0.

First of all, we consider the case of the Gaussian distribution. In Figure 5 we show the noise reduction factor as a function of the standard deviation σ_0 for different values of t_0. Even if, in general, σ_0 can assume values larger than 1, in our analysis we explored only values in the interval (0,1) since they are sufficient to observe the degradation of nonclassicality. The data, shown as colored dots + error bars, are superimposed to the theoretical fitting curves that can be obtained according to Equation (4), in which we fix the values of $\langle m\rangle$ and η and leave m_μ and $t_{0,\mathrm{FIT}}$ as fitting parameters. In particular, we set $\langle m\rangle = 2.23$, which is the maximum value of the mean number of photons detected in the variable arm, and $\eta = 0.145$, which is the quantum efficiency of the detection chain obtained as $\eta = 1 - R_{MIN}$, being R_{MIN} the value of the noise reduction factor corresponding to $t = 1$. In the fitting procedure, we leave $t_{0,\mathrm{FIT}}$ as a free fitting parameter to take into account the possibility that the preparation of the distribution of t is not ideal due to the discrete values of t at our disposal. By inspecting panel (a) of Figure 5, we notice that the smaller the mean value the more difficult the observation of nonclassicality. Indeed, for $t_0 = 0.4$ only small values of σ_0 make the condition $R < 1$ possible. On the contrary, for $t_0 = 0.9$ the chance to observe nonclassicality is higher.

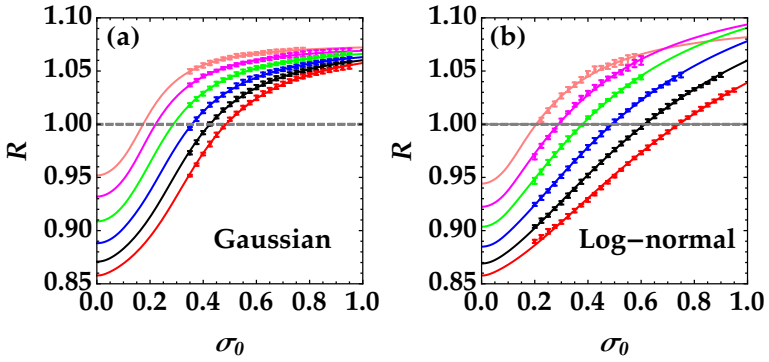

Figure 5. Noise reduction factor as a function of the standard deviation σ_0 of the Gaussian (panel (**a**)) and log-normal (panel (**b**)) distributions defined over the entire domain for different values of t_0. The experimental data are shown as colored dots + error bars: pink dots refer to $t_0 = 0.4$, magenta dots to $t_0 = 0.5$, green dots to $t_0 = 0.6$, blue dots to $t_0 = 0.7$, black dots to $t_0 = 0.8$, and red dots to $t_0 = 0.9$. The corresponding theoretical fitting functions are plotted as colored curves with the same color choice. In the fitting procedure we fixed $\langle m \rangle = 2.23$ and $\eta = 0.145$ and we left $t_{0,\mathrm{FIT}}$ and m_μ as fitting parameters. The values of such parameters are reported in Tables 1 and 2 together with the χ^2 per degree of freedom.

The behavior exhibited by the noise reduction factor in the case of the log-normal distribution, shown in panel (b) of Figure 5, is quite similar. Indeed, also in this case, observing the nonclassicality is particularly difficult for small values of t_0. However, it is interesting to notice that, at variance with the Gaussian distribution, for large values of t_0 the values of R linearly increase as a function of σ_0, while for small values the behavior is more similar to a sigmoid. The different behavior of R for different choices of t_0 is due to the nontrivial and asymmetric shape of the log-normal distribution at different mean values, as already shown in Figure 2. The fitting parameters corresponding to the data shown in Figure 5 are summarized in Table 1 for the Gaussian distributions and in Table 2 for the log-normal ones. In particular, we note that the fitted values of m_μ are almost constant in the case of Gaussian distributions, while they change in the case of log-normal ones.

Table 1. Values of the fitting parameters $t_{0,\mathrm{FIT}}$ and m_μ of the noise reduction factor as a function of σ_0 for $\langle m \rangle = 2.23$ and $\eta = 0.145$ in the case of Gaussian distributions of t. In the last column the χ^2 per degree of freedom is shown.

t_0	$t_{0,\mathrm{FIT}}$	m_μ	χ^2_ν
0.4	0.460 ± 0.002	0.2171 ± 0.0007	0.018
0.5	0.523 ± 0.002	0.2115 ± 0.0007	0.060
0.6	0.616 ± 0.002	0.2115 ± 0.0008	0.054
0.7	0.721 ± 0.002	0.213 ± 0.001	0.118
0.8	0.839 ± 0.003	0.217 ± 0.002	0.198
0.9	0.964 ± 0.003	0.226 ± 0.002	0.463

Table 2. Values of the fitting parameters $t_{0,\mathrm{FIT}}$ and m_μ of the noise reduction factor as a function of σ_0 for $\langle m \rangle = 2.23$ and $\eta = 0.145$ in the case of log-normal distributions of t. In the last column the χ^2 per degree of freedom is shown.

t_0	$t_{0,\mathrm{FIT}}$	m_μ	χ^2_ν
0.4	0.369 ± 0.007	0.077 ± 0.004	0.418
0.5	0.508 ± 0.007	0.126 ± 0.006	0.784
0.6	0.618 ± 0.004	0.161 ± 0.005	0.423
0.7	0.734 ± 0.002	0.189 ± 0.003	0.309
0.8	0.852 ± 0.002	0.213 ± 0.003	0.346
0.9	0.964 ± 0.003	0.226 ± 0.006	0.697

4. Discussion

The different behavior of the mean number of photons per mode for the two distributions can be ascribed to the fact that, when the mean number of photons is varied in one arm of the twin beam, also the number of modes changes. Indeed, the number of modes we obtain from the first two moments of the light statistics is an "effective" one describing the multimode state as the tensor product of μ equally-populated single-mode states. This is just a useful approximation since in the real experiment the different modes are differently populated [35]. For this reason, the attenuation of light by a filter (the HWP followed by the PBS is equivalent to such a condition) can vary the number of effective modes since some of the real modes can be so attenuated to go below the detection threshold. In particular, we experimentally observed that the number of effective modes monotonically increases at increasing the values of the mean number of photons. The variability of the number of modes is amplified when the data are combined according to specific distributions of t. As discussed above, this is more visible in the case of log-normal distribution due to its nontrivial shape at different mean values.

To better investigate the role played by the mean number of photons per mode in the calculation of the noise reduction factor for the two considered distributions, we theoretically study the behavior of R as a function of σ_0 by properly fixing the parameters appearing in Equation (4). In particular, we set $\langle m \rangle = 2.23$, $\eta = 0.145$ and consider two possible values of m_μ, 0.1 and 0.04. The resulting expressions for R are plotted in Figure 6.

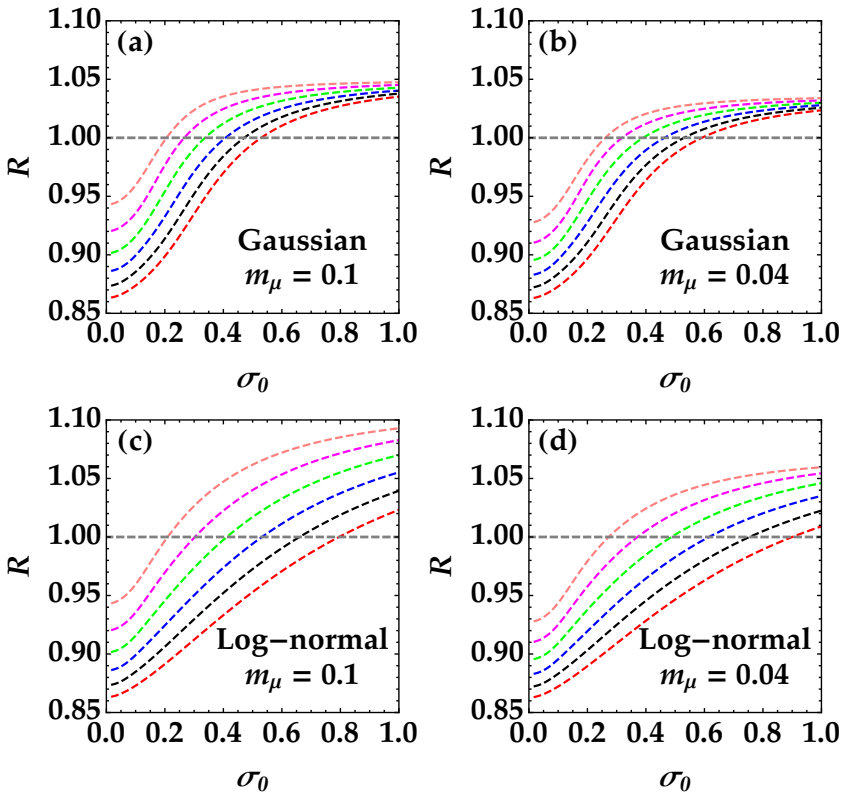

Figure 6. Theoretical values of the noise reduction factor as a function of the standard deviation σ_0 of the Gaussian (panels (**a**,**b**)) and log-normal (panels (**c**,**d**)) distributions for different values of t_0. For all the shown curves we set $\langle m \rangle = 2.23$, $\eta = 0.145$. In panels (**a**,**c**) $m_\mu = 0.1$, while in panel (**b**,**d**) $m_\mu = 0.04$. In each panel, the pink curve corresponds to $t_0 = 0.4$, the magenta curve to $t_0 = 0.5$, the green curve to $t_0 = 0.6$, the blue curve to $t_0 = 0.7$, the black curve to $t_0 = 0.8$ and the red curve to $t_0 = 0.9$.

We note that the choice $\langle m \rangle = 2.23$, and $m_\mu = 0.1$ corresponds to a twin-beam state with $\sim$22 modes, while $\langle m \rangle = 2.23$, and $m_\mu = 0.04$ corresponds to a twin-beam state with $\sim$56 modes, which represents a more reliable experimental condition than the first choice.

The curves shown in panels (a) and (b) are for Gaussian distributions, while those in panels (c) and (d) are for log-normal distributions. In general, the plots resemble the experimental behavior of the plots in Figure 5. However, we notice that depending on the choice of m_μ, the value of σ_0 at which the noise reduction factor is equal to 1, namely the boundary between classical and nonclassical correlations, changes. In particular, the lower the value of m_μ, the larger the threshold value of σ_0. Indeed, according to Equation (4), the lower the value of m_μ, the lower the value of R. To better investigate this result, in Figure 7 we plot the values of σ_0 at which, for fixed choices of $\langle m \rangle$ and η and for 4 possible choices of m_μ, the theoretical value of R is equal to 1 as a function of t_0. We show the results in the case of Gaussian distributions in panel (a) and those for log-normal distributions in panel (b). In general, we can see that the threshold values of σ_0 increase at increasing values of t_0 with different slopes for the two distributions. Moreover, for log-normal distributions of t the growth is more rapid than for Gaussian distributions.

The direct comparison among the curves corresponding to the same kind of distribution leads us to conclude that reducing the mean number of photons per mode, that is increasing the number of modes, makes it possible the detection of nonclassical correlations in the case of wider distributions of t, that is for a highly fluctuating transmittance of the communication channel. Thus, a proper tailoring of the mode structures of the state can make the employed twin beam more robust to losses. We also notice that all the results achieved so far encourage us to test our optical states in more realistic situations. Indeed, as reported in Ref. [20], the probability distributions of t corresponding to free-space quantum channels under diverse weather conditions are characterized by mean values that range from 0.9 down to 0.3. In some cases, the model that describes the transmission efficiency is more symmetric thus resembling a Gaussian distribution, whereas in other situations is more similar to a log-normal distribution.

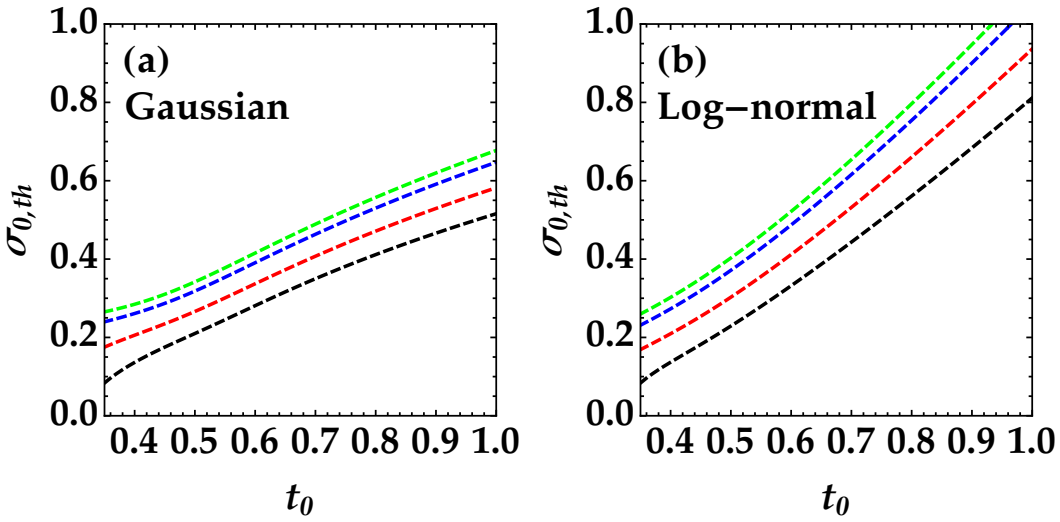

Figure 7. Expected threshold value of σ_0 obtained by setting $R = 1$ in Equation (4) for $\langle m \rangle = 2.23$ and $\eta = 0.145$. The data are shown as a function of t_0 for different choices of m_μ: 0.2 (black curve), 0.1 (red curve), 0.04 (blue curve) and 0.02 (green curve). Panel (**a**) corresponds to the case of Gaussian distributions of t_0, while panel (**b**) to the case of log-normal distributions.

5. Conclusions

In this paper we explored the survival of nonclassical correlations between the parties of mesoscopic twin-beam states propagating through an asymmetric lossy channel, in which the transmission coefficient was statistically distributed. In particular, we considered the case of Gaussian

distributions and that of log-normal ones. We investigated the role played by the parameters characterizing the light (mean number of photons and mean number of photons per mode), the transmission channel (mean value and standard deviation of the distribution) and the detection chain (quantum efficiency). In general, we can conclude, as expected, that the larger the mean value of the distribution the better the observation of nonclassicality. Moreover, at a given mean value of the distribution, the larger its standard deviation the worse the observation of nonclassicality. In general, these results hold for both the Gaussian and the log-normal distributions. Not surprisingly, the different shape of the distributions is responsible for the different behavior for the same choice of parameters. In addition, we studied the dependence of the robustness of sub-shot-noise correlations undergoing a statistically distributed amount of loss on the number of modes. We found that high multimode twin-beam states are more robust to loss than low-multimode ones. This result can be ascribed to the fact that a twin beam endowed with many modes has a photon-number distribution less thermal, and thus less fluctuating, than a single-mode one [36–38]. Such a result suggests that, in order to optimize the propagation of light in the presence of loss, a proper tailoring of the employed quantum state should be performed in advance.

Author Contributions: Both authors equally contributed to each step of the work. All authors have read and agreed to the published version of the manuscript.

Funding: This research received no external funding.

Acknowledgments: A. A. acknowledges the Project "Investigating the effect of noise sources in the free-space transmission of mesoscopic quantum states of light" supported by the University of Insubria.

Conflicts of Interest: The authors declare no conflict of interest.

Abbreviations

The following abbreviations are used in this manuscript:

HWP	Half-wave plate
PBS	Polarizing cube beam splitter

References

1. Bennett, C.H.; Bessette, F.; Brassard, G.; Salvail, L.; Smolin, J. Experimental Quantum Cryptography. *J. Cryptol.* **1992**, *5*, 3–28. [CrossRef]
2. Muller, A.; Zbinden, H.; Gisin, N. Underwater quantum coding. *Nature* **1995**, *378*, 449. [CrossRef]
3. Marcikic, I.; de Riedmatten, H.; Tittel, W.; Zbinden, H.; Gisin, N. Long-distance teleportation of qubits at telecommunication wavelengths. *Nature* **2003**, *421*, 509–513. [CrossRef] [PubMed]
4. Ursin, R.; Jennewein, T.; Aspelmeyer, M.; Kaltenbaek, R.; Lindenthal, M.; Walther, P.; Zeilinger, A. Communications: Quantum teleportation across the Danube. *Nature* **2004**, *430*, 849. [PubMed]
5. Kurtsiefer, C.; Zarda, P.; Halder, M.; Weinfurter, H.; Gorman, P.M.; Tapster, P.R.; Rarity, J.G. A step towards global key distribution. *Nature* **2002**, *419*, 450. [CrossRef] [PubMed]
6. Aspelmeyer, M.; Böhm, H.R.; Gyatso, T.; Jennewein, T.; Kaltenbaek, R.; Lindenthal, M.; Molina-Terriza, G.; Poppe, A.; Resch, K.; Taraba, M.; et al. Long-Distance Free-Space Distribution of Quantum Entanglement. *Science* **2003**, *301*, 621. [CrossRef]
7. Jin, X.M.; Ren, J.G.; Yang, B.; Yi, Z.H.; Zhou, F.; Xu, X.F.; Wang, S.K.; Yang, D.; Hu, Y.F.; Jiang, S.; et al. Experimental free-space quantum teleportation. *Nat. Photon.* **2010**, *4*, 376–381. [CrossRef]
8. Capraro, I.; Tomaello, A.; Dall'Arche, A.; Gerlin, F.; Ursin, R.; Vallone, G.; Villoresi, P. Impact of turbulence in long range quantum and classical communications. *Phys. Rev. Lett.* **2012**, *109*, 200502.
9. Peuntinger, C.; Heim, B.; Müller, C.R.; Gabriel, C.; Marquardt, C.; Leuchs, G. Distribution of squeezed states through an atmospheric channel. *Phys. Rev. Lett.* **2014**, *113*, 060502. [CrossRef]
10. Vallone, G.; Bacco, D.; Dequal, D.; Gaiarin, S.; Luceri, V.; Bianco, G.; Villoresi, P. Experimental Satellite Quantum Communications. *Phys. Rev. Lett.* **2015**, *115*, 040502. [CrossRef]

11. Carrasco-Casado, A.; Kunimori, H.; Takenaka, H.; Kubo-Oka, T.; Akioka, M.; Fuse, T.; Koyama, Y.; Kolev, D.; Munemasa, Y.; Toyoshima, M. LEO-to-ground polarization measurements aiming for space QKD using Small Optical TrAnsponder (SOTA). *Opt. Express* **2016**, *24*, 12254. [CrossRef] [PubMed]
12. Dequal, D.; Vidarte, L.T.; Rodriguez, V.R.; Vallone, G.; Villoresi, P.; Leverrier, A.; Diamanti, E. Feasibility of satellite-to-ground continuous-variable quantum key distribution. *arXiv* **2020**, arXiv:2002.02002.
13. Semenov, A.A.; Vogel, W. Quantum light in the turbulent atmosphere. *Phys. Rev. A* **2009**, *80*, 021802(R). [CrossRef]
14. Usenko, V.C.; Heim, B.; Peuntinger, C.; Wittmann, C.; Marquardt, C.; Leuchs, G.; Filip, R. Entanglement of Gaussian states and the applicability to quantum key distribution over fading channels. *New J. Phys.* **2012**, *14*, 093048. [CrossRef]
15. Bohmann, M.; Kruse, R.; Sperling, J.; Silberhorn, C.; Vogel, W. Probing free-space quantum channels with laboratory-based experiments. *Phys. Rev. A* **2017**, *95*, 063801. [CrossRef]
16. Michálek, V.; Perina, J., Jr.; Haderka, O. Experimental Quantification of the Entanglement of Noisy Twin Beams. *Phys. Rev. Appl.* **2020**, *14*, 024003.
17. Allevi, A.; Bondani, M. Preserving nonclassical correlations in strongly unbalanced conditions. *J. Opt. Soc. Am. B* **2019**, *36*, 3275–3281. [CrossRef]
18. Straka, I.; Mika, J.; Ježek, M. Generator of arbitrary classical photon statistics. *Opt. Express* **2018**, *26*, 8998–9010. [CrossRef]
19. Milonni, P.W.; Carter, J.H.; Peterson, C.G.; Hughes, R.J. Effects of propagation through atmospheric turbulence on photon statistics. *J. Opt. B Quantum Semiclass. Opt.* **2004**, *6*, S742–S745. [CrossRef]
20. Vasylyev, D.; Semenov, A.A.; Vogel, W.; Günthner, K.; Thurn, A.; Bayraktar, Ö.; Marquardt, C. Free-space quantum links under diverse weather conditions. *Phys. Rev. A* **2017**, *96*, 043856.
21. Agliati, A.; Bondani, M.; Andreoni, A.; De Cillis, G.; Paris M.G.A. Quantum and classical correlations of intense beams of light via joint photodetection. *J. Opt. B* **2005**, *7*, 652 . [CrossRef]
22. Lee, C.T. Many-photon antibunching in generalized pair coherent states. *Phys. Rev. A* **1990**, *41*, 1569. [CrossRef] [PubMed]
23. Lee, C.T. Nonclassical photon statistics of two-mode squeezed states. *Phys. Rev. A* **1990**, *42*, 1608. [CrossRef] [PubMed]
24. Peres, A. Separability criterion for density matrices. *Phys. Rev. Lett.* **1996**, *77*, 1413. [CrossRef]
25. Simon, R. Peres-Horodecki Separability Criterion for Continuous Variable Systems. *Phys. Rev. Lett.* **2000**, *84*, 2726. [CrossRef]
26. Richter, T.; Vogel, W. Nonclassicality of quantum states: A hierarchy of observable conditions. *Phys. Rev. Lett.* **2002**, *89*, 283601. [CrossRef]
27. Degiovanni, I.P.; Genovese, M.; Schettini, V.; Bondani, M.; Andreoni, A.; Paris, M.G.A. Monitoring the quantum-classical transition in thermally seeded parametric down-conversion by intensity measurements. *Phys. Rev. A* **2009**, *79*, 063836. [CrossRef]
28. Allevi, A.; Olivares, S.; Bondani, M. Measuring high-order photon-number correlations in experiments with multimode pulsed quantum states. *Phys. Rev. A* **2012**, *85*, 063835. [CrossRef]
29. Brida, G.; Genovese, M.; Ruo Berchera, I. Experimental realization of sub-shot-noise quantum imaging. *Nat. Photon.* **2010**, *4*, 227–230.
30. Chan, K.W.; O'Sullivan, M.N.; Boyd, R.W. High-order thermal ghost imaging. *Opt. Lett.* **2009**, *34*, 3343–3345. [CrossRef]
31. Bondani, M.; Allevi, A.; Andreoni, A. Ghost imaging by intense multimode twin beam. *Eur. Phys. J. Spec. Top.* **2012**, *203*, 151–161. [CrossRef]
32. Allevi, A.; Bondani, M. Can nonclassical correlations survive in the presence of asymmetric lossy channels? *Eur. Phys. J. D* **2018**, *72*, 178. [CrossRef]
33. Allevi, A.; Bondani, M. Nonlinear and Quantum Optical Properties and Applications of Intense Twin-Beams. *Adv. At. Mol. Opt. Phys.* **2017**, *66*, 49–110.
34. Bondani, M.; Allevi, A.; Agliati, A.; Andreoni, A. Self-consistent characterization of light statistics. *J. Mod. Opt.* **2009**, *56*, 226–231. [CrossRef]
35. Allevi, A.; Lamperti, M.; Bondani, M.; Peřina, J., Jr.; Michálek, V.; Haderka, O.; Machulka, R. Characterizing the nonclassicality of mesoscopic optical twin-beam states. *Phys. Rev. A* **2013**, *88*, 063807. [CrossRef]

36. Lamperti, M.; Allevi, A.; Bondani, M.; Machulka, R.; Michálek, V.; Haderka, O.; Peřina, J., Jr. Optimal sub-Poissonian light generation from twin beams by photon-number resolving detectors. *J. Opt. Soc. Am. B* **2014**, *31*, 20–25.
37. Allevi, A.; Bondani, M. Statistics of twin-beam states by photon-number resolving detectors up to pump depletion. *J. Opt. Soc. Am. B* **2014**, *31*, B14–B19. [CrossRef]
38. Arkhipov, I.I.; Peřina, J., Jr.; Peřina, J.; Miranowicz, A. Comparative study of nonclassicality, entanglement, and dimensionality of multimode noisy twin beams. *Phys. Rev. A* **2015**, *91*, 033837. [CrossRef]